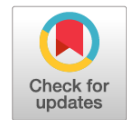


DOI: <https://doi.org/10.17816/DD633391>

EDN: QXLAWR



Comparison of the Diagnostic Accuracy of Whole-Body Diffusion-Weighted Imaging and ¹⁸F-Prostate-Specific Membrane Antigen-1007 Positron Emission Tomography Combined with Computed Tomography for Detecting Bone Metastases in Prostate Cancer

Pavel B. Gelezhe^{1,2}, Roman V. Reshetnikov¹, Ivan A. Blokhin¹, Maria R. Kodenko¹¹ Research and Practical Clinical Center for Diagnostics and Telemedicine Technologies, Moscow, Russia;² European Medical Center, Moscow, Russia

ABSTRACT

BACKGROUND: The increasing availability of ¹⁸F-prostate-specific membrane antigen-1007 (¹⁸F-PSMA-1007) for prostate cancer staging highlighted its advantages, particularly its higher spatial resolution compared to analogs. Moreover, accumulating scientific data indicate an increase in false-positive findings, predominantly in bones, which may lead to unwarranted upstaging of the disease. Diffusion-weighted imaging may be used for the early detection of bone metastases.

AIM: This study aimed to assess and compare the diagnostic accuracy of whole-body ¹⁸F-PSMA-1007 positron emission tomography combined with computed tomography and whole-body and pelvic bone diffusion-weighted imaging in patients with prostate cancer.

METHODS: A retrospective single-center selective study was conducted. The imaging results of 119 patients with prostate cancer were divided into two groups: group 1 comprised 40 pairs of ¹⁸F-PSMA-1007 positron emission tomography combined with computed tomography and whole-body diffusion-weighted magnetic resonance imaging scans, and group 2 included 79 pairs of similar studies, with magnetic resonance imaging performed only for the pelvic bones. The diagnostic studies were performed at an inter-study interval ≤ 14 days. The metastatic bone lesions detected in different anatomical regions was counted using data from ¹⁸F-PSMA-1007 positron emission tomography combined with computed tomography and magnetic resonance imaging. Lesions were considered true positives if confirmed by additional magnetic resonance imaging pulse sequences and/or follow-up observation.

RESULTS: Whole-body diffusion-weighted imaging demonstrated higher specificity (58.1%) for detecting bone metastases than ¹⁸F-PSMA-1007 positron emission tomography combined with computed tomography (51.06%). However, its sensitivity was lower: 93.22% versus 97.55%.

CONCLUSION: Despite its advantages, ¹⁸F-PSMA-1007 positron emission tomography combined with computed tomography shows a high rate of false-positive bone findings. These are most commonly noted in the ribs, vertebrae, and pelvic bones. Suspicious bone lesions should be further evaluated to avoid unjustified disease upstaging. Thus, whole-body magnetic resonance imaging with diffusion-weighted sequences and selective fat signal suppression can be used.

Keywords: prostate-specific membrane antigen; positron emission tomography; magnetic resonance imaging; diffusion-weighted imaging; prostate cancer.

To cite this article:

Gelezhe PB, Reshetnikov RV, Blokhin IA, Kodenko MR. Comparison of the Diagnostic Accuracy of Whole-Body Diffusion-Weighted Imaging and ¹⁸F-Prostate-Specific Membrane Antigen-1007 Positron Emission Tomography Combined with Computed Tomography for Detecting Bone Metastases in Prostate Cancer. *Digital Diagnostics*. 2025;6(2):239–250. DOI: 10.17816/DD633391 EDN: QXLAWR

Submitted: 10.06.2024

Accepted: 06.12.2024

Published online: 05.06.2025

DOI: <https://doi.org/10.17816/DD633391>

EDN: QXLAWR

Сравнительная оценка диагностической точности диффузионно-взвешенных изображений всего тела и позитронно-эмиссионной томографии с ^{18}F -простатоспецифичным мембранным антигеном-1007, совмещённой с компьютерной томографией, в выявлении костных метастазов при раке предстательной железы

П.Б. Гележе^{1,2}, Р.В. Решетников¹, И.А. Блохин¹, М.Р. Коденко¹¹ Научно-практический клинический центр диагностики и телемедицинских технологий, Москва, Россия;² Европейский медицинский центр, Москва, Россия

АННОТАЦИЯ

Обоснование. Повышение доступности ^{18}F -простатоспецифичного мембранного антигена-1007 (^{18}F -ПСМА-1007) для стадирования рака предстательной железы демонстрирует его преимущества, из которых важным является более высокое пространственное разрешение, чем у аналогов. Одновременно накапливаются научные данные, свидетельствующие о значительном увеличении числа ложноположительных находок, преимущественно в костях, что может приводить к необоснованному завышению стадии онкологического процесса. Диффузионно-взвешенные изображения возможно использовать для ранней диагностики метастатического поражения костей.

Цель исследования. Оценка диагностической точности позитронно-эмиссионной томографии всего тела с ^{18}F -ПСМА-1007, совмещённой с компьютерной томографией (ПЭТ/КТ), в сравнении с диффузионно-взвешенными изображениями всего тела и костей малого таза у пациентов с раком предстательной железы.

Методы. Проведено ретроспективное одноцентровое выборочное исследование. Результаты исследований 119 пациентов с раком предстательной железы, разделены на две группы: 1-я группа — 40 пар данных ПЭТ/КТ с ^{18}F -ПСМА-1007 и магнитно-резонансной томографии с диффузионно-взвешенными изображениями всего тела; 2-я группа — 79 пар аналогичных исследований, при этом магнитно-резонансную томографию проводили только в области костей таза. Диагностические исследования выполнены при соблюдении временного интервала между ними не более 14 дней. Осуществляли подсчёт количества выявленных метастатических очагов костей в различных анатомических областях по данным ПЭТ/КТ с ^{18}F -ПСМА-1007 и магнитно-резонансной томографии. Истинно положительными считают очаги, подтверждённые с помощью дополнительных импульсных последовательностей магнитно-резонансной томографии и/или в результате динамического наблюдения.

Результаты. Диффузионно-взвешенная визуализация всего тела продемонстрировала более высокую специфичность в выявлении костных метастазов (58,1%) по сравнению с ПЭТ/КТ с ^{18}F -ПСМА-1007 (51,06%). Однако чувствительность оказалась ниже — 93,22 против 97,55% соответственно.

Заключение. Несмотря на известные преимущества, ПЭТ/КТ с ^{18}F -ПСМА-1007 демонстрирует высокую частоту ложноположительных находок в костях. Наиболее частая их локализация — рёбра, позвонки, кости таза. Для избежания неоправданного завышения стадии рекомендуется проведение уточняющей диагностики подозрительных очагов костей. В качестве такого метода можно использовать магнитно-резонансную томографию всего тела с диффузионно-взвешенными изображениями и селективным подавлением сигнала от жировой ткани.

Ключевые слова: простатоспецифичный мембранный антиген; позитронно-эмиссионная томография; магнитно-резонансная томография; диффузионно-взвешенные изображения; рак предстательной железы.

Как цитировать:

Гележе П.Б., Решетников Р.В., Блохин И.А., Коденко М.Р. Сравнительная оценка диагностической точности диффузионно-взвешенных изображений всего тела и позитронно-эмиссионной томографии с ^{18}F -простатоспецифичным мембранным антигеном-1007, совмещённой с компьютерной томографией, в выявлении костных метастазов при раке предстательной железы // Digital Diagnostics. 2025. Т. 6, № 2. С. 239–250. DOI: 10.17816/DD633391 EDN: QXLAWR

Рукопись получена: 10.06.2024

Рукопись одобрена: 06.12.2024

Опубликована online: 05.06.2025

DOI: <https://doi.org/10.17816/DD633391>

EDN: QXLAWR

弥散加权全身成像与¹⁸F-前列腺特异性膜抗原-1007正电子发射计算机断层显像联合计算机断层扫描在前列腺癌骨转移检测中的诊断准确性比较评估

Pavel B. Gelezhe^{1,2}, Roman V. Reshetnikov¹, Ivan A. Blokhin¹, Maria R. Kodenko¹¹ Research and Practical Clinical Center for Diagnostics and Telemedicine Technologies, Moscow, Russia;² European Medical Center, Moscow, Russia

摘要

论证。随着¹⁸F-前列腺特异性膜抗原-1007 (¹⁸F-PSMA-1007) 在前列腺癌分期中的应用日益普及, 其更高的空间分辨率逐渐显现出相对于其他同类示踪剂的优势。与此同时, 越来越多研究指出, 该示踪剂主要在骨组织中导致大量假阳性发现, 从而可能引起肿瘤分期的不合理升高。弥散加权成像可作为骨转移早期诊断的一种方法。

目的: 评估¹⁸F-PSMA-1007全身正电子发射计算机断层显像联合计算机断层扫描 (PET/CT) 在前列腺癌患者中, 与全身及骨盆区域弥散加权成像相比, 在骨转移检出方面的诊断准确性。

方法。本研究为一项回顾性、单中心抽样研究。共纳入119例前列腺癌患者的检查结果, 并将其分为两组: 第1组为40对¹⁸F-PSMA-1007 PET/CT与全身弥散加权成像磁共振检查数据; 第2组为79对类似检查数据, 其中磁共振检查仅限于骨盆区域。所有诊断性检查均在时间间隔不超过14天的前提下完成。根据¹⁸F-PSMA-1007 PET/CT和磁共振成像的结果, 统计不同解剖部位检测到的骨转移灶数量。以磁共振成像的额外脉冲序列和/或动态随访结果作为依据, 确认的病灶被视为真阳性。

结果。全身弥散加权成像在骨转移检出方面的特异性为58.1%, 高于¹⁸F-PSMA-1007 PET/CT的51.06%。但敏感性略低, 分别为93.22%和97.55%。

结论。尽管¹⁸F-PSMA-1007 PET/CT具有已知优势, 但在骨骼中显示出较高的假阳性检出率。其最常见的累及部位为肋骨、椎骨和骨盆骨。为避免肿瘤分期被不当地提高, 建议对可疑骨骼病灶进行进一步评估。可采用全身磁共振成像, 结合弥散加权成像和选择性脂肪信号抑制序列, 作为此类补充诊断方法。

关键词: 前列腺特异性膜抗原; 正电子发射计算机断层显像; 磁共振成像; 弥散加权成像; 前列腺癌。

引用本文:

Gelezhe PB, Reshetnikov RV, Blokhin IA, Kodenko MR. 弥散加权全身成像与¹⁸F-前列腺特异性膜抗原-1007正电子发射计算机断层显像联合计算机断层扫描在前列腺癌骨转移检测中的诊断准确性比较评估. *Digital Diagnostics*. 2025;6(2):239–250. DOI: 10.17816/DD633391 EDN: QXLAWR

收到: 10.06.2024

接受: 06.12.2024

发布日期: 05.06.2025

BACKGROUND

Positron emission tomography/computed tomography (PET/CT) with prostate-specific membrane antigen (PSMA)-targeting radiopharmaceuticals is increasingly widely used in clinical practice for prostate cancer staging. PET/CT has become the preferred approach in the diagnosis of biochemical recurrence in prostate cancer [1, 2]. Several clinical studies have confirmed that PET/CT with PSMA-targeting radiopharmaceuticals outperforms magnetic resonance imaging (MRI), CT, and radiolabeled choline in detecting biochemical recurrence [3, 4]. Furthermore, PSMA improves the accuracy of primary staging in intermediate- and high-risk prostate cancer [5].

In the United States and Europe, gallium-68 is the most commonly used isotope in PSMA-targeting radiopharmaceuticals. Specifically, ^{68}Ga -PSMA-11 was the first PET radiopharmaceutical approved in the United States for patients with prostate cancer [6]. With advancements in radiopharmacy, ^{18}F -PSMA ligands, such as ^{18}F -PSMA-1007, have become widely used.

The main technical advantages of ^{18}F -PSMA ligands over ^{68}Ga -PSMA include a longer half-life (110 min vs. 68 min) and the possibility of cyclotron production. Moreover, ^{18}F -PSMA has lower positron emission energy than ^{68}Ga -PSMA (0.6 MeV vs. 2.3 MeV), increasing the spatial resolution of phantom scans [7]. Another advantage of ^{18}F -PSMA-1007 is the radiopharmaceutical's low background activity in the urinary tract [8].

However, as ^{18}F -PSMA-1007 becomes more widely used, reports of false-positive findings in bones increase [9]. This can lead to an unreasonable overestimation of the disease stage, resulting in an ineffective treatment strategy.

The key advantages of MRI, which was introduced as a diagnostic tool several decades ago, include excellent soft tissue contrast and the absence of radiation exposure.

Diffusion-weighted imaging (DWI) is an MRI mode that measures the microscopic movement of water molecules at the cellular level. DWI provides both quantitative (e.g., apparent diffusion coefficient) and qualitative (e.g., signal intensity) data for the differential diagnosis of benign and malignant neoplasms [10].

DWI was initially used in brain diseases, including to detect cerebral infarction zones based on diffusion restriction. Technical advances introduced in the late 1990s, such as diffusion-weighted imaging with background suppression (DWIBS), made it possible to use DWI to diagnose extracranial disorders. The key advantage of DWIBS is quick, free-breathing whole-body imaging, which opens up new prospects for cancer staging [10].

However, given its low resolution, DWIBS alone is insufficiently effective. The fundamental advantage of DWIBS is that it detects lesions based on high signal intensity at high b values [11]. To accurately determine the anatomic site of the detected lesion, whole-body DWI

must be supplemented by basic MRI sequences, such as T1 weighted images (T1WI), short tau inversion recovery (STIR), and some others [12].

DWI is currently used to visualize metastases. Malignant tumors typically have a more intense DWI signal than benign ones. Diffusion restriction by tumor tissues may be caused by a greater number of cells per unit volume, resulting in smaller intercellular spaces. The advantages of whole-body DWI include a short scan time (approximately 20 minutes), no ionizing radiation, and no need for intravenous contrast. Furthermore, DWI is a clarifying MRI sequence in whole-body examinations in cancer, including the diagnosis of distant metastases [13].

AIM

The work aimed to assess the diagnostic accuracy of whole-body PET/CT with ^{18}F -PSMA-1007 compared to whole-body and pelvic DWI in patients with prostate cancer.

METHODS

Study Design

A retrospective, single-center study was conducted.

Eligibility Criteria

Inclusion criteria:

- Prostate cancer with signs of biochemical recurrence;
- Multiparametric prostate MRI;
- Whole-body DWI;
- Whole-body PET/CT with ^{18}F -PSMA-1007;
- Interval between MRI and PET of no more than 14 days.

Non-inclusion criteria: absence of one or more diagnostic markers of prostate cancer.

Exclusion criteria: significant artifacts of pelvic DWI, whole-body DWI, or whole-body PET/CT with ^{18}F -PSMA-1007, preventing proper assessment of findings.

Study Setting

Patients who underwent PET/CT with ^{18}F -PSMA-1007, whole-body DWI, and prostate MRI were enrolled at the private healthcare facility European Medical Center.

Study Duration

The study used electronic medical records obtained between January 1, 2023, and June 1, 2023.

Intervention

Two datasets were generated at the first stage of the study:

- PET/CT with ^{18}F -PSMA-1007 and whole-body DWI;
- PET/CT with ^{18}F -PSMA-1007 and pelvic DWI.

The interval between MRI and PET was no more than 14 days.

At the second stage, the number of metastatic bone lesions at various anatomic sites was assessed using PET with ^{18}F -PSMA-1007 and MRI findings.

A Biograph[®] mCT scanner (Siemens Healthineers, Germany) was used for PET/CT with ^{18}F -PSMA-1007. Whole-body (head-to-toes) PET/CT was performed. The radiopharmaceutical activity was calculated as 3.0–4.0 MBq per 1 kg body weight (mean: 250–350 MBq). After receiving the radiopharmaceutical, patients rested for 60 minutes. Oral hydration with 500 mL of water was performed. The scan time per axial field of view (the area corresponding to the patient's position on the scanner bed) was 3 minutes.

PSMA-RADS-3,¹ PSMA-RADS-4,² and PSMA-RADS-5³ lesions are classified as doubtful or positive based on PET findings [14]. To be classified as true-positive, a lesion must be confirmed by additional MRI sequences, including:

- Axial in-phase and out-of-phase T1WIs, HASTE T2WIs,⁴ and sagittal T1WIs of the spine for whole-body MRI findings;
- Axial in-phase and out-of-phase T1WIs, HASTE T2WIs,⁴ and dynamic contrast-enhanced T1WIs for pelvic MRI findings [15].

The scanning used a head coil, two flexible body coils, and a spine coil. The overall scan time was determined by the patient's anthropometric characteristics, but did not exceed 50 minutes. Table 1 shows protocols for prostate MRI and whole-body DWI.

Main Study Outcome

Detection of metastatic bone lesions using PET/CT with ^{18}F -PSMA-1007 and whole-body and pelvic diffusion-weighted imaging findings, confirmed by additional MRI sequences.

Subgroup Analysis

All findings were divided into two groups:

- Group 1: PET/CT with ^{18}F -PSMA-1007 and whole-body DWI findings;
- Group 2: PET/CT with ^{18}F -PSMA-1007 and pelvic DWI findings.

Outcomes Registration

The number of detected lesions was entered into a table, indicating the anatomic site. To assess the distribution by anatomic sites, metastases to cranial bones, scapulas, ribs, pelvic bones, and vertebrae were counted individually.

Table 1. Protocols of whole-body and prostate diffusion-weighted magnetic resonance imaging

MRI sequence	Slice orientation	TE/TR, ms	Field of view, mm	Slice thickness, mm / overlap, %
<i>Multiparametric magnetic resonance imaging of the prostate</i>				
TSE T2-weighted image	Sagittal	120/3800	250×250	3/0.3
TSE T2-weighted image	Axial	110/3938	180×180	2.5/0
SS-EPI diffusion-weighted image	Axial	87/2425	160×160	3/0.3
SS-EPI diffusion-weighted image	Axial	59/5400	200×200	3/0
TSE T2-weighted image	Coronal	110/2500	160×160	2.5/0
Dynamic contrast-enhanced T1-weighted image, temporal resolution 15 s	Axial	2.3/4.6	250×250	3/0
T1-weighted image after contrast enhancement	Axial	1.3/2.3	400×350	4/0
<i>Whole-body diffusion-weighted magnetic resonance imaging</i>				
SS-EPI diffusion-weighted image	Axial	76/15 600	380×285	5/0
TSE T1-weighted image	Sagittal	12/630	340×340	4/0
HASTE T2-weighted image	Axial	91/1400	385×313	6/0
VIBE DIXON T1-weighted image	Axial	6.69/2.39–4.77	380×309	4/
TIRM T2-weighted image	Axial	86/7200	230×201	5/0

Note. TSE, turbo spin echo; SS-EPI, single-shot echo planar imaging; HASTE, half-Fourier acquisition single-shot turbo spin echo; VIBE DIXON, volumetric interpolated breath-hold examination with the Dixon method; TIRM, turbo inversion recovery magnitude; TE, echo time; TR, repetition time.

¹ PSMA-RADS-3 (Prostate-Specific Membrane Antigen Reporting and Data System 3): equivocal malignancy requiring further evaluation, according to the standardized system for interpretation of imaging findings obtained with radiopharmaceuticals.

² PSMA-RADS-4 (Prostate-Specific Membrane Antigen Reporting and Data System 4): high likelihood of malignancy, according to the standardized system for interpretation of imaging findings obtained with radiopharmaceuticals.

³ PSMA-RADS-5 (Prostate-Specific Membrane Antigen Reporting and Data System 5): very high likelihood of malignancy; high probability of clinically significant cancer, according to the standardized system for interpretation of imaging findings obtained with radiopharmaceuticals.

⁴ HASTE (Half-Fourier Acquisition Single-shot Turbo Spin Echo): a rapid sequence that enables acquisition of the entire image in a single radiofrequency pulse.

Moreover, metastases to pelvic bones were counted individually for whole-body and pelvic MRI findings.

Each lesion detected using PET/CT with ^{18}F -PSMA-1007 and whole-body and pelvic DWI findings was compared with a reference test (MRI scans with additional MRI sequences). Only lesions that met the diagnostic criteria for metastases based on additional MRI sequences were classified as true-positive. The additional MRI sequences included frequency-selective fat suppression (in-phase and out-of-phase T1WIs) for reliable detection of a metastatic lesion and a red marrow reconversion zone [16, 17].

Ethics Approval

The study was approved by the Independent Ethics Committee of the Center for Diagnostics and Telemedicine (Minutes No. 10/2023 dated December 21, 2023).

Statistical Analysis

Sample size calculation

Given the lack of data for accurately predicting expected effects, the sample size was calculated using the estimated average effect size of 0.5 [18]. According to the Altman nomogram, with the effect size of 0.5, significance level of 0.05, and power of 0.8, the required sample size will be 120 patients [19].

Statistical methods

The diagnostic accuracy of the studied techniques was assessed by calculating their sensitivity and specificity.

- Sensitivity (Se) was assessed as the proportion of true-positive findings:

$$Se = \frac{TP}{TP+FN}, \quad (1)$$

where TP is the number of true-positive findings; FN is the number of false-negative findings.

- Specificity (Sp) was assessed as the proportion of true-negative findings:

$$Sp = \frac{TN}{TN+FP}, \quad (2)$$

where TN is the number of true-negative findings; FP is the number of false-positive findings.

The number of true-positive findings was defined as the number of lesions at the examined anatomic site, confirmed by additional MRI sequences. The number of true-negative findings was defined as the number of patients without lesions at the examined anatomic site according to index and reference tests. If the number of lesions at the examined anatomic site based on the index test exceeded the number based on the reference test, the difference was regarded the number of false-positive findings. Otherwise, the difference was interpreted as the number of false-negative findings. The sensitivity and specificity of each index test for each anatomic site are shown with 95% confidence intervals (CIs). The overall sensitivity and specificity of each index test are presented as means and interquartile ranges. The McNemar's test was used to compare index and reference tests.

R 4.2.1⁵ was used for all calculations [20].

RESULTS

Participants

The study included findings for 119 patients:

Group 1: 40 data pairs of PET/CT with ^{18}F -PSMA-1007 and whole-body DWI findings;

Group 2: 79 data pairs of PET/CT with ^{18}F -PSMA-1007 and pelvic DWI findings.

Table 2 shows the total number of metastatic lesions in group 1, confirmed by additional MRI sequences.

Table 3 shows the total number of metastatic lesions in group 2, confirmed by additional MRI sequences. In addition to bone metastases, group 2 showed signs of prostate cancer recurrence near the vesicourethral anastomosis in 31 patients and signs of pelvic lymph node involvement in 59 patients. In group 1, signs of recurrence near the vesicourethral anastomosis were

Table 2. Number of metastatic bone lesions detected in group 1

Anatomic site	PET/CT with ^{18}F -PSMA-1007, n	Whole-body DWI, n	Lesions confirmed by other MRI sequences, n
Skull	53	50	35
Scapulas	59	55	46
Ribs	240	218	167
Vertebrae	225	220	176
Pelvis	135	131	114
Extremities	22	29	20

Note. PET/CT, positron emission tomography/computed tomography; PSMA, prostate-specific membrane antigen; DWI, diffusion-weighted image; MRI, magnetic resonance imaging.

⁵ R 4.2.1 [Internet]. R: The R Project for Statistical Computing; 2022. Available at: <https://www.r-project.org/>. Accessed on: April 10, 2024.

Table 3. Number of metastatic lesions detected in group 2

Anatomic site	PET/CT with ¹⁸ F-PSMA-1007, <i>n</i>	Whole-body DWI, <i>n</i>	Lesions confirmed by other MRI sequences, <i>n</i>
Pelvis	118	80	79
Extremities	30	18	18

Note. PET/CT, positron emission tomography/computed tomography; PSMA, prostate-specific membrane antigen; DWI, diffusion-weighted image; MRI, magnetic resonance imaging.

found in 17 patients, and signs of retroperitoneal and pelvic lymph node involvement in 28 patients.

Primary Results

The distribution (%) of metastatic lesions by anatomic sites was as follows:

- 12.5% in cranial bones
- 42.5% in the spine
- 27.5% in the ribs
- 17.5% in the scapulas
- 42.5% in pelvic bones, and
- 17.5% in the extremities.

The maximum sensitivity and specificity of whole-body DWI were 93.22 (95% CI: 87.67–97.81) and 58.10% (95% CI: 31.54–74.62), respectively. The maximum sensitivity and specificity of whole-body PET/CT with ¹⁸F-PSMA-1007 were 97.55 (95% CI: 95.13–100.00) and 51.06% (95% CI: 20.35–76.59), respectively. Table 4 shows the calculated diagnostic parameters for selected anatomic sites. In group 2, the sensitivity was 100% for both techniques, whereas the sensitivity was 85.18% for whole-body PET/CT with ¹⁸F-PSMA-1007 and 100% for pelvic DWI (see Table 5).

DISCUSSION

Summary of Primary Results

The main study outcome is a relatively low specificity of both PET/CT with ¹⁸F-PSMA-1007 and whole-body DWI in detecting bone metastases. Pelvic DWI obtained by multiparametric prostate MRI showed higher specificity. Whole-body DWI showed the highest specificity in detecting skull, scapula, and femur metastases.

Discussion of Primary Results

The findings indicate low specificity of PET/CT with ¹⁸F-PSMA-1007 and whole-body DWI in detecting bone metastases, which is confirmed by recent clinical studies, including multicenter studies. Grünig et al. [21] reported that PET/CT with ¹⁸F-PSMA-1007 detected hyperfixation foci in bones in 51.4% of patients, which are difficult to interpret due to their unclear origin. One of the first published works comparing the diagnostic accuracy of PET/CT with ¹⁸F-PSMA-1007 and ⁶⁸Ga-PSMA-11 found significant differences in false positive rates in the bones (48% vs. 14.7%). This is traditionally explained by the longer half-life of ¹⁸F compared to ⁶⁸Ga, which increases spatial resolution and

Table 4. Diagnostic accuracy parameters in group 1

Anatomic site	PET/CT with ¹⁸ F-PSMA-1007		Whole-body DWI		χ^2	<i>p</i> -value
	Se, % (95% CI)	Sp, % (95% CI)	Se, % (95% CI)	Sp, % (95% CI)		
Skull	100 (90.11–100)	64 (50.14–75.86)	100 (90.11–100)	69.39 (55.47–80.48)	0.129	0.720
Scapulas	100 (91.62–100)	63.83 (49.54–76.03)	91.3 (71.68–96.57)	71.11 (56.63–82.27)	0.800	0.372
Ribs	98.74 (95.53–99.65)	19.42 (12.94–28.1)	98.74 (95.53–99.65)	31.46 (22.75–41.7)	3.645	0.057
Vertebrae	95.93 (91.84–98.01)	20 (12.51–30.41)	95.93 (91.84–98.01)	27.63 (18.84–38.58)	0.275	0.601
Pelvis	96.36 (91.02–98.58)	38.3 (25.79–52.57)	96.36 (91.02–98.58)	46.81 (33.33–60.77)	0.444	0.505
Extremities	94.44 (74.24–99.01)	85.29 (69.87–93.55)	94.44 (74.24–99.01)	72.09 (57.31–83.25)	4.455	0.035

Note. PET/CT, positron emission tomography/computed tomography; PSMA, prostate-specific membrane antigen; DWI, diffusion-weighted image; Se, sensitivity; Sp, specificity; CI, confidence interval; χ^2 , McNemar's test.

Table 5. Diagnostic accuracy parameters in group 2

Anatomic site	PET/CT with ¹⁸ F-PSMA-1007		Whole-body DWI		χ^2	<i>p</i> -value
	Se, % (95% CI)	Sp, % (95% CI)	Se, % (95% CI)	Sp, % (95% CI)		
Таз	98.73 (93.17–99.78)	52.94 (42.43–63.19)	100 (95.36–100)	98.28 (90.86–99.69)	35.103	<0.001
Конечности	100 (82.41–100)	85.19 (75.87–91.32)	100 (82.41–100)	100 (95–100)	11.000	<0.001

Note. PET/CT, positron emission tomography/computed tomography; PSMA, prostate-specific membrane antigen; DWI, diffusion-weighted image; Se, sensitivity; Sp, specificity; CI, confidence interval; χ^2 , McNemar's test.

improves signal-to-noise ratio [9]. Immunohistochemistry found PSMA not only in prostate tissues, but also in inflammation and neoangiogenesis foci [22]. Furthermore, PSMA-based radiopharmaceuticals can target benign bone lesions (see Fig. 1), such as red marrow hyperplasia, which is frequently detected in the ribs [23] and vertebral hemangiomas [24]. The interpretation of magnetic resonance images of vertebral hemangiomas is rarely challenging, and they are easily distinguished from prostate cancer metastases. However, atypical hemangiomas frequently require histological confirmation [25]. The exact mechanism of PSMA-based radiopharmaceutical fixation in benign bone lesions is unknown.

Restricted diffusion in benign lesions, such as red marrow reconversion zones, is a significant challenge for radiologists when interpreting bone DWI findings. T1-weighted Dixon MRI sequences with frequency-selective fat suppression can be used for differential diagnosis of these lesions [26, 27]. Furthermore, degenerative changes in the spine are frequently associated with signs of restricted diffusion (see Fig. 2). MRI sequences with frequency-selective fat suppression reliably detect metastases and Schmorl's nodes [28].

Whole-body DWI is widely used in primary staging of cancers with high risk for bone metastases, including prostate cancer. According to Hottat et al. [29], the diagnostic accuracy in detecting bone metastases can

reach 92%. Whole-body DWI is not inferior to PET/CT with ^{18}F -choline and outperforms bone scintigraphy in detecting bone metastases in prostate cancer [30]. A meta-analysis by Liu et al. demonstrated comparable diagnostic accuracy of PET/CT with ^{68}Ga -PSMA and whole-body MRI [31]. Furthermore, international publications indicate that whole-body DWI alone can be used to detect bone metastases [32]. Sun et al. [33] conducted a study in patients with different cancers and reported comparable sensitivity, as well as positive and negative prognostic value, of whole-body DWI and PET/CT with ^{18}F -fluorodeoxyglucose. The diffusion coefficient in benign bone lesions was significantly higher than in metastases. Combined rapid free-breathing MRI sequences without contrast are widely used for cancer staging in all body systems. A combination of T1WI, STIR, and DWI is typically used. Larbi et al. [34] compared different combinations of MRI sequences for detecting bone metastases in prostate cancer and found that the diagnostic value of T1WI + DWI was comparable to that of T1WI + STIR.

We found significant ($p < 0.001$) differences in diagnostic accuracy between whole-body PET/CT with ^{18}F -PSMA-1007 and pelvic DWI, which could be attributed to the broader field of view in pelvic DWI (see Table 1). According to Park et al. [27], pelvic DWI allowed for the differentiation of pelvic bone metastases in prostate cancer from benign lesions, with significant differences.

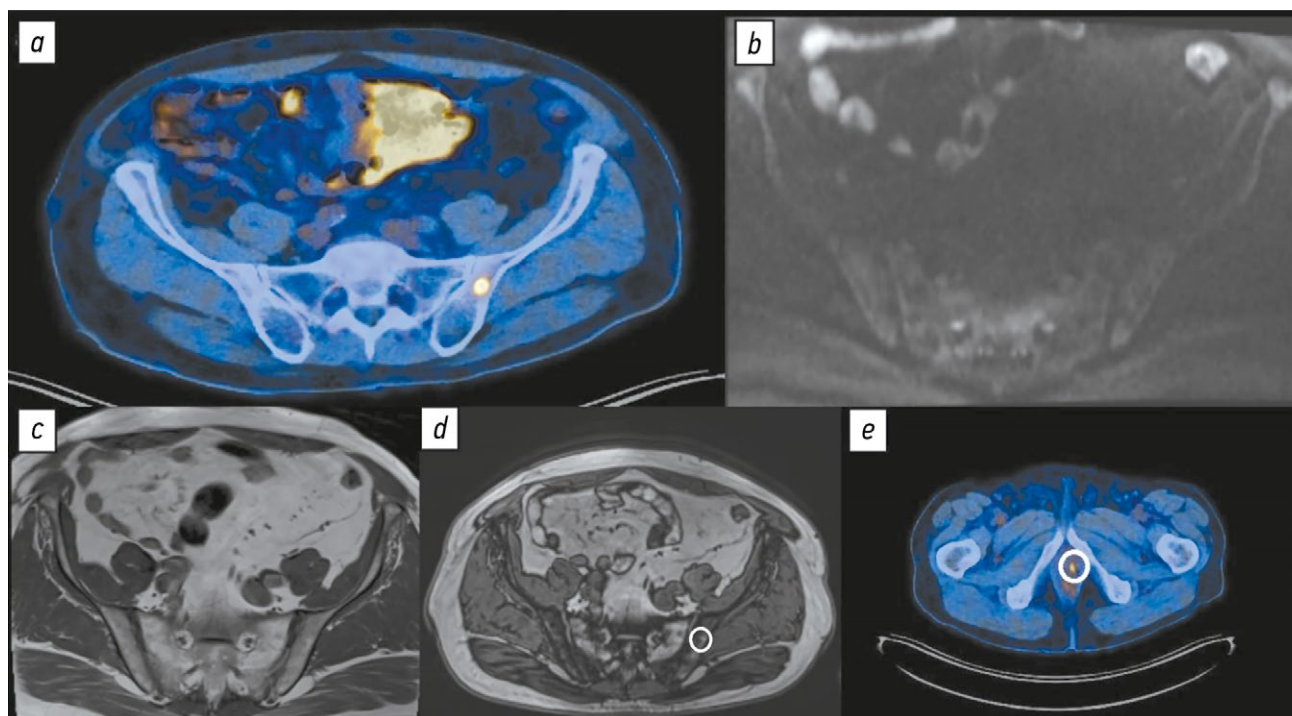


Fig. 1. Patient A., 56 years old, with mixed neuroendocrine prostate cancer T3aN1Mx, Gleason 8 (4 + 4). Condition after radical prostatectomy. Total serum prostate-specific antigen elevated to 1.87 ng/mL. Tumor recurrence near the vesicourethral anastomosis: *a*, axial positron emission tomography/computed tomography scan: a radiopharmaceutical hyperfixation focus in the left ilium, suspicious for metastasis; *b* and *c*, no focal lesions in the left ilium according to diffusion-weighted (*b*) and T1-weighted images without fat suppression (*c*); *d*, a signal void corresponding to red marrow reconversion in the radiopharmaceutical hyperfixation focus according to the T1-weighted image, without abnormal bone marrow infiltration; *e*, a hyperfixation focus near the vesicourethral anastomosis according to positron emission tomography/computed tomography with ^{18}F -prostate-specific membrane antigen-1007.

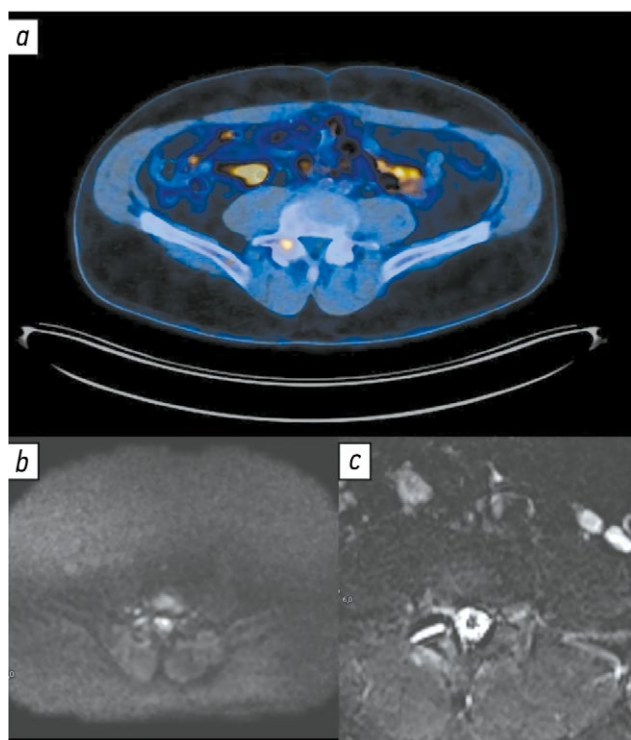


Fig. 2. Patient B., 77 years old, with prostate adenocarcinoma T4N2M0, Gleason 8 (4 + 4). Condition after comprehensive treatment, several lines of hormone therapy, chemotherapy, and radiotherapy of the prostate and regional lymph nodes. Total serum prostate-specific antigen elevated to 0.4 ng/mL. Example of a false-positive finding: *a*, axial positron emission tomography/computed tomography with ^{18}F -prostate-specific membrane antigen-1007: a radiopharmaceutical hyperfixation focus in the right LV arch, suspicious for metastasis; *b* and *c*, — diffusion-weighted (*b*) and T2-weighted magnetic resonance images (*c*): signs of arthritis of the right LV-SI facet joint with joint effusion and moderate trabecular edema of adjacent articular surfaces.

Study Limitations

There is currently no non-invasive gold standard for the compared techniques, making it difficult to eliminate the effect of concordant findings on the results [21, 35, 36]. Notably, multiparametric MRI is not the preferred method for detecting bone metastases; therefore, the use of other MRI sequences as a reference test to assess the diagnostic accuracy of PET/CT with ^{18}F -PSMA-1007 and DWI is a significant limitation of this study. Histological confirmation of all identified metastatic lesions is impossible for technical reasons. However, the approach used in this study is frequently applied in international research. For example, Freitag et al. [37] and Chen et al. [35] assessed the concordance between the findings.

This retrospective study only included patients with confirmed prostate cancer; therefore, the distribution

of normal and abnormal findings in the sample did not match the actual distribution in this patient population. Whole-body DWI, which was used to clarify the nature of suspicious findings obtained by PET/CT with ^{18}F -PSMA-1007, did not rule out the radiologist's bias in assessing the identified lesions.

CONCLUSION

Despite its well-known advantages, PET/CT with ^{18}F -PSMA-1007 has high false positive rates in the bones, primarily the ribs, vertebrae, and pelvic bones. DWI cannot be used alone to clarify doubtful findings of PET/CT with ^{18}F -PSMA-1007. Multiparametric whole-body MRI is recommended to prevent unreasonable overestimation of the disease stage.

ADDITIONAL INFORMATION

Author contributions: P.B. Gelezhe, R.V. Reshetnikov: conceptualization, formal analysis, writing—original draft, writing—review & editing; I.A. Blokhin, M.R. Kodenko: formal analysis, writing—original draft, writing—review & editing. All the authors approved the version of the manuscript to be published and agreed to be accountable for all aspects of the work, ensuring that questions related to the accuracy or integrity of any part of the work are appropriately investigated and resolved.

Ethics approval: The study was approved by the Independent Ethics Committee of State Budget-Funded Health Care Institution of the City of Moscow Research and Practical Clinical Center for Diagnostics and Telemedicine Technologies of the Moscow Health Care Department (Meeting Minutes No. 10/2023 dated December 21, 2023).

Consent for publication: All patients signed a written informed consent form that included a clause on the possible publication of anonymized data, including diagnostic images, for scientific purposes.

Funding sources: This article is part of the research project Opportunistic Screening for Socially Significant and Other Common Diseases (Unified State Information Accounting System No. 123031400009-1), in accordance with Order No. 1196 dated December 21, 2022, On Approval of State Assignments Funded by the Budget of the City of Moscow for State Budgetary (Autonomous) Institutions Under the Jurisdiction of the Moscow City Health Department for 2023 and the Planned Period of 2024–2025, issued by the Moscow City Health Department.

Disclosure of interests: The authors have no relationships, activities, or interests for the last three years related to for-profit or not-for-profit third parties whose interests may be affected by the content of the article.

Statement of originality: No previously published material (text, images, or data) was used in this work.

Data availability statement: The editorial policy regarding data sharing does not apply to this work.

Generative AI: No generative artificial intelligence technologies were used to prepare this article.

Provenance and peer review: This paper was submitted unsolicited and reviewed following the standard procedure. The peer review process involved an external reviewer, two members of the editorial board, and the in-house science editor.

REFERENCES | СПИСОК ЛИТЕРАТУРЫ

- Petersen LJ, Zacho HD. PSMA PET for primary lymph node staging of intermediate and high-risk prostate cancer: an expedited systematic review. *Cancer Imaging*. 2020;20(1):1–8. doi: 10.1186/s40644-020-0290-9 EDN: EWACNH
- Wongergem M, van der Zant FM, Broos WAM, Knol RJJ. Clinical impact of PSMA PET in biochemically recurrent prostate cancer; a review of the literature. *Tijdschrift voor Urologie*. 2020;10(6-7):109–121. doi: 10.1007/s13629-020-00296-6 EDN: XRLHSC

3. Hofman MS, Lawrentschuk N, Francis RJ, et al. Prostate-specific membrane antigen PET-CT in patients with high-risk prostate cancer before curative-intent surgery or radiotherapy (proPSMA): a prospective, randomised, multicentre study. *The Lancet*. 2020;395(10231):1208–1216. doi: 10.1016/s0140-6736(20)30314-7 EDN: IDQIFB
4. Treglia G, Annunziata S, Pizzuto DA, et al. Detection rate of 18F-Labeled PSMA PET/CT in biochemical recurrent prostate cancer: a systematic review and a meta-analysis. *Cancers*. 2019;11(5):710. doi: 10.3390/cancers11050710
5. Donswijk ML, van Leeuwen PJ, Vegt E, et al. Clinical impact of PSMA PET/CT in primary prostate cancer compared to conventional nodal and distant staging: a retrospective single center study. *BMC Cancer*. 2020;20(1):1–10. doi: 10.1186/s12885-020-07192-7 EDN: QXMNJJ
6. The FDA approves PSMA-targeted drug for PET imaging in men with prostate cancer. *BJU International*. 2021;127(3):267–268. doi: 10.1111/bju.15361
7. Caribé PRRV, Koole M, D'Asseler Y, et al. NEMA NU 2-2007 performance characteristics of GE Signa integrated PET/MR for different PET isotopes. *EJNMMI Physics*. 2019;1(6):11. doi: 10.1186/s40658-019-0247-x
8. Giesel FL, Hadaschik B, Cardinale J, et al. F-18 labelled PSMA-1007: biodistribution, radiation dosimetry and histopathological validation of tumor lesions in prostate cancer patients. *European Journal of Nuclear Medicine and Molecular Imaging*. 2016;44(4):678–688. doi: 10.1007/s00259-016-3573-4 EDN: RQYCMY
9. Kroenke M, Mirzoyan L, Horn T, et al. Matched-pair comparison of 68Ga-PSMA-11 and 18F-rhPSMA-7 PET/CT in patients with primary and biochemical recurrence of prostate cancer: frequency of non-tumor-related uptake and tumor positivity. *Journal of Nuclear Medicine*. 2020;62(8):1082–1088. doi: 10.2967/jnumed.120.251447 EDN: EQTOAN
10. Kwee TC, Takahara T, Ochiai R, et al. Diffusion-weighted whole-body imaging with background body signal suppression (DWIBS): features and potential applications in oncology. *European Radiology*. 2008;18(9):1937–1952. doi: 10.1007/s00330-008-0968-z EDN: BJSYMC
11. Parker C, Tunariu N, Tovey H, et al. Radium-223 in metastatic castration-resistant prostate cancer: whole-body diffusion-weighted magnetic resonance imaging scanning to assess response. *JNCI Cancer Spectrum*. 2023;7(6):pkad077. doi: 10.1093/jncics/pkad077 EDN: AZWTFB
12. Dresen RC, De Vuysere S, De Keyzer F, et al. Whole-body diffusion-weighted MRI for operability assessment in patients with colorectal cancer and peritoneal metastases. *Cancer Imaging*. 2019;19(1):1–10. doi: 10.1186/s40644-018-0187-z EDN: IEYSWA
13. Yamamoto S, Yoshida S, Ishii C, et al. Metastatic diffusion volume based on apparent diffusion coefficient as a prognostic factor in castration-resistant prostate cancer. *Journal of Magnetic Resonance Imaging*. 2021;54(2):401–408. doi: 10.1002/jmri.27596 EDN: SFBHRH
14. Rowe SP, Pienta KJ, Pomper MG, Gorin MA. PSMA-RADS Version 1.0: a step towards standardizing the interpretation and reporting of PSMA-targeted PET imaging studies. *European Urology*. 2018;73(4):485–487. doi: 10.1016/j.eururo.2017.10.027
15. Vasilev YA, Omelyanskaya OV, Vladzmyrskyy AV, et al. Comparison of multiparametric and biparametric magnetic resonance imaging protocols for prostate cancer diagnosis by radiologists with different experience. *Digital Diagnostics*. 2023;4(4):455–466. doi: 10.17816/dd322816 EDN: PVEPWX
16. Disler DG, McCauley TR, Ratner LM, et al. In-phase and out-of-phase MR imaging of bone marrow: prediction of neoplasia based on the detection of coexistent fat and water. *American Journal of Roentgenology*. 1997;169(5):1439–1447. doi: 10.2214/ajr.169.5.9353477
17. Suh CH, Yun SJ, Jin W, et al. Diagnostic Performance of in-phase and opposed-phase chemical-shift imaging for differentiating benign and malignant vertebral marrow lesions: a meta-analysis. *American Journal of Roentgenology*. 2018;211(4):W188–W197. doi: 10.2214/AJR.17.19306
18. Halpern SD. The continuing unethical conduct of underpowered clinical trials. *JAMA*. 2002;288(3):358–362. doi: 10.1001/jama.288.3.358
19. Altman DG. Statistics and ethics in medical research: III How large a sample? *BMJ*. 1980;281(6251):1336–1338. doi: 10.1136/bmj.281.6251.1336
20. Blokhin IA, Kodenko MR, Shumskaya YuF, et al. Hypothesis testing using R. *Digital Diagnostics*. 2023;4(2):238–247. doi: 10.17816/DD121368 EDN: OEK DAG
21. Grünig H, Maurer A, Thali Y, et al. Focal unspecific bone uptake on [18F]-PSMA-1007 PET: a multicenter retrospective evaluation of the distribution, frequency, and quantitative parameters of a potential pitfall in prostate cancer imaging. *European Journal of Nuclear Medicine and Molecular Imaging*. 2021;48(13):4483–4494. doi: 10.1007/s00259-021-05424-x
22. Silver DA, Pellicer I, Fair WR, et al. Prostate-specific membrane antigen expression in normal and malignant human tissues. *Clin Cancer Res*. 1997;3(1):81–85.
23. Plouznikoff N, Garcia C, Artigas C, et al. Heterogeneity of 68Ga-PSMA PET/CT uptake in fibrous dysplasia. *Clinical Nuclear Medicine*. 2019;44(10):e593–e594. doi: 10.1097/RLU.0000000000002609
24. Gossili F, Lyngby CG, Løgager V, Zacho HD. Intense PSMA uptake in a vertebral hemangioma mimicking a solitary bone metastasis in the primary staging of prostate cancer via 68Ga-PSMA PET/CT. *Diagnostics*. 2023;13(10):1730. doi: 10.3390/diagnostics13101730 EDN: HQPGMR
25. Hoyle JM, Layfield LJ, Crim J. The lipid-poor hemangioma: an investigation into the behavior of the “atypical” hemangioma. *Skeletal Radiology*. 2020;49:93–100. doi: 10.1007/s00256-019-03257-2
26. Liao Z, Liu G, Ming B, et al. Evaluating prostate cancer bone metastasis using accelerated whole-body isotropic 3D T1-weighted Dixon MRI with compressed SENSE: a feasibility study. *European Radiology*. 2023;33(3):1719–1728. doi: 10.1007/s00330-022-09181-9
27. Park S, Park JG, Jun S, et al. Differentiation of bone metastases from prostate cancer and benign red marrow depositions of the pelvic bone with multiparametric MRI. *Magnetic Resonance Imaging*. 2020;73:118–124. doi: 10.1016/j.mri.2020.08.019 EDN: CTHKSL
28. Lee JH, Park S. Differentiation of schmorl nodes from bone metastases of the spine: use of apparent diffusion coefficient derived from DWI and fat fraction derived from a Dixon sequence. *American Journal of Roentgenology*. 2019;213(5):W228–W235. doi: 10.2214/AJR.18.21003
29. Hottat NA, Badr DA, Ben Ghanem M, et al. Assessment of whole-body MRI including diffusion-weighted sequences in the initial staging of breast cancer patients at high risk of metastases in comparison with PET-CT: a prospective cohort study. *European Radiology*. 2023;34(1):165–178. doi: 10.1007/s00330-023-10060-0 EDN: MRFKJM
30. Johnston EW, Latifoltojar A, Sidhu HS, et al. Multiparametric whole-body 3.0-T MRI in newly diagnosed intermediate- and high-risk prostate cancer: diagnostic accuracy and interobserver agreement for nodal and metastatic staging. *European Radiology*. 2018;29(6):3159–3169. doi: 10.1007/s00330-018-5813-4 EDN: DEXLFX
31. Liu F, Dong J, Shen Y, et al. Comparison of PET/CT and MRI in the diagnosis of bone metastasis in prostate cancer patients: a network analysis of diagnostic studies. *Frontiers in Oncology*. 2021;11(APR):736654. doi: 10.3389/fonc.2021.736654 EDN: TKTQOV
32. Nakanishi K, Tanaka J, Nakaya Y, et al. Whole-body MRI: detecting bone metastases from prostate cancer. *Japanese Journal of Radiology*. 2021;40(3):229–244. doi: 10.1007/s11604-021-01205-6 EDN: QZBDSB
33. Sun W, Li M, Gu Y, et al. Diagnostic value of whole-body DWI with background body suppression plus calculation of apparent diffusion coefficient at 3 T Versus 18F-FDG PET/CT for detection of bone metastases. *American Journal of Roentgenology*. 2020;214(2):446–454. doi: 10.2214/ajr.19.21656 EDN: BJRCLP
34. Larbi A, Omoumi P, Pasoglou V, et al. Whole-body MRI to assess bone involvement in prostate cancer and multiple myeloma: comparison of the diagnostic accuracies of the T1, short tau inversion recovery (STIR), and high b-values diffusion-weighted imaging (DWI) sequences. *European Radiology*. 2018;29(8):4503–4513. doi: 10.1007/s00330-018-5796-1 EDN: CEOKNS
35. Chen B, Wei P, Macapinlac HA, Lu Y. Comparison of 18F-Fluciclovine PET/CT and 99mTc-MDP bone scan in detection of bone metastasis in prostate cancer. *Nuclear Medicine Communications*. 2019;40(9):940–946. doi: 10.1097/MNM.0000000000001051 EDN: ZRPGWP
36. Gelezhe P.B. *Comprehensive diagnostics of breast cancer using magnetic resonance imaging and positron emission tomography with 18F-fluorodeoxyglucose, combined with computed tomography* [dissertation]. Moscow; 2020. Available from: <https://www.elibrary.ru/item.asp?id=54413422> EDN: UGEBZO
37. Freitag MT, Radtke JP, Hadaschik BA, et al. Comparison of hybrid 68Ga-PSMA PET/MRI and 68Ga-PSMA PET/CT in the evaluation of lymph node and bone metastases of prostate cancer. *European Journal of Nuclear Medicine and Molecular Imaging*. 2015;43(1):70–83. doi: 10.1007/s00259-015-3206-3 EDN: HXYHGT

AUTHORS' INFO

* **Pavel B. Gelezhe**, MD, Cand. Sci. (Medicine);
address: 24 Petrovka st, Moscow, Russia, 127051;
ORCID: 0000-0003-1072-2202;
eLibrary SPIN: 4841-3234;
e-mail: gelezhe.pavel@gmail.com

Roman V. Reshetnikov, Cand. Sci. (Physics and Mathematics);
ORCID: 0000-0002-9661-0254;
eLibrary SPIN: 8592-0558;
e-mail: ReshetnikovRV1@zdrav.mos.ru

Ivan A. Blokhin, MD, Cand. Sci. (Medicine);
ORCID: 0000-0002-2681-9378;
eLibrary SPIN: 3306-1387;
e-mail: BlokhinIA@zdrav.mos.ru

Maria R. Kodenko, Cand. Sci. (Engineering);
ORCID: 0000-0002-0166-3768;
eLibrary SPIN: 5789-0319;
e-mail: KodenkoM@zdrav.mos.ru

ОБ АВТОРАХ

* **Гележе Павел Борисович**, канд. мед. наук;
адрес: Россия, 127051, Москва, ул. Петровка 24;
ORCID: 0000-0003-1072-2202;
eLibrary SPIN: 4841-3234;
e-mail: gelezhe.pavel@gmail.com

Решетников Роман Владимирович, канд. физ.-мат. наук;
ORCID: 0000-0002-9661-0254;
eLibrary SPIN: 8592-0558;
e-mail: ReshetnikovRV1@zdrav.mos.ru

Блохин Иван Андреевич, канд. мед. наук;
ORCID: 0000-0002-2681-9378;
eLibrary SPIN: 3306-1387;
e-mail: BlokhinIA@zdrav.mos.ru

Коденко Мария Романовна, канд. техн. наук;
ORCID: 0000-0002-0166-3768;
eLibrary SPIN: 5789-0319;
e-mail: KodenkoM@zdrav.mos.ru

* Corresponding author / Автор, ответственный за переписку